Single Sheet Functionalized Graphene by Oxidation and Thermal Expansion of Graphite

Michael J. McAllister,[†] Je-Luen Li,[‡,§,||] Douglas H. Adamson,[§] Hannes C. Schniepp,[†] Ahmed A. Abdala,[†,⊥] Jun Liu,[⊗,○] Margarita Herrera-Alonso,[†] David L. Milius,[†] Roberto Car,[‡,§] Robert K. Prud'homme,[†] and Ilhan A. Aksay*[,†]

Department of Chemical Engineering, Department of Chemistry, and Princeton Institute for the Science and Technology of Materials, Princeton University, Princeton, New Jersey 08544, and Sandia National Laboratories, Albuquerque, New Mexico 87185

Received December 26, 2006. Revised Manuscript Received February 6, 2007

A detailed analysis of the thermal expansion mechanism of graphite oxide to produce functionalized graphene sheets is provided. Exfoliation takes place when the decomposition rate of the epoxy and hydroxyl sites of graphite oxide exceeds the diffusion rate of the evolved gases, thus yielding pressures that exceed the van der Waals forces holding the graphene sheets together. A comparison of the Arrhenius dependence of the reaction rate against the calculated diffusion coefficient based on Knudsen diffusion suggests a critical temperature of 550 °C which must be exceeded for exfoliation to occur. As a result of their wrinkled nature, the functionalized and defective graphene sheets do not collapse back to graphite oxide but are highly agglomerated. After dispersion by ultrasonication in appropriate solvents, statistical analysis by atomic force microscopy shows that 80% of the observed flakes are single sheets.

Introduction

Graphene, the basal plane of graphite, is composed of a honeycomb arrangement of carbon atoms and is the basis of carbon nanotubes (CNTs).[1,2] Graphene single sheets are expected to have tensile modulus and ultimate strength values similar to those of single wall carbon nanotubes (SWCNTs)[3] and are also electrically conducting.[4] Much like SWCNTs,[5] graphene sheets serve as fillers for the enhancement of mechanical[6] and electrical properties[7] in composite materials. Recent studies in which single sheets of graphene have been prepared by the removal of one sheet at a time by a "Scotch tape" method have shown promising electrical properties that could be useful for developing novel electronic devices.[4,8−12] Motivated by the promise of graphene as an alternative to SWCNTs, in a recent study[13] we reported a method to produce functionalized single graphene sheets (FGSs) in bulk quantities through thermal expansion of graphite oxide (GO). In this report, we provide a detailed analysis of the expansion mechanism and a detailed characterization of the resultant material.

Starting with Brodie[14] in 1859, there has been an extensive body of literature concerning graphite and graphite modification.[15−21] GO formation involves the reaction of graphite

* Corresponding author: e-mail iaksay@princeton.edu.
[†] Department of Chemical Engineering, Princeton University.
[‡] Department of Chemistry, Princeton University.
[§] Princeton Institute for the Science and Technology of Materials, Princeton University.
[||] Current address: Institute of Atomic and Molecular Sciences, Academia Sinica, Taipei 10617, Taiwan.
[⊥] Current address: Department of Chemical Engineering, The Petroleum Institute, POB 2533, Abu Dhabi, United Arab Emirates.
[⊗] Sandia National Laboratories.
[○] Current address: Pacific Northwest National Laboratory, Richland, Washington 99352.

(1) Iijima, S. *Nature* **1991**, *354*, 56.
(2) Ajayan, P. M.; Iijima, S. *Nature* **1993**, *361*, 333.
(3) Ab initio calculations by Je-Luen Li and Roberto Car (Princeton University) showed that the stress−strain behaviors of graphene sheets and SWCNTs are very similar. The calculated Young's modulus is 1.01 TPa for graphene sheet and 0.94−0.96 TPa for SWCNT provided the same graphene sheet thickness (0.34 nm) is used.
(4) Novoselov, K. S.; Geim, A. K.; Morozov, S. V.; Jiang, D.; Zhang, Y.; Dubonos, S. V.; Grigorieva, I. V.; Firsov, A. A. *Science* **2004**, *306*, 666.
(5) Ramanathan, T.; Liu, H.; Brinson, L. C. *J. Polym. Sci., Part B: Polym. Phys.* **2005**, *43*, 2269.
(6) Ramanathan, T.; Abdala, A. A.; Stankovich, S.; Dikin, D. A.; Herrera-Alonso, M.; Piner, R. D.; Adamson, D. H.; Liu, J.; Chen, X.; Ruoff, R. S.; Nguyen, S. T.; Aksay, I. A.; Prud'homme, R. K.; Brinson, L. C., unpublished.
(7) Stankovich, S.; Dikin, D. A.; Dommett, G. H. B.; Kohlhaas, K. M.; Zimney, E. J.; Stach, E. J.; Piner, R. D.; Nguyen, S. T.; Ruoff, R. S. *Nature* **2006**, *442*, 282.
(8) Duplock, E. J.; Scheffler, M.; Lindan, P. J. D. *Phys. Rev. Lett.* **2004**, *92*, 225502.
(9) Novoselov, K. S.; Jiang, D.; Schedin, F.; Booth, T. J.; Khothevich, V. V.; Morozov, S. V.; Geim, A. K. *Proc. Natl. Acad. Sci. U.S.A.* **2005**, *102*, 10451.
(10) Zhang, Y.; Tan, Y. W.; Stormer, H. L.; Kim, P. *Nature* **2005**, *438*, 201.
(11) Zhang, Y.; Small, J. P.; Amori, M. E. S.; Kim, P. *Phys. Rev. Lett.* **2005**, *94*, 176803.
(12) Novoselov, K. S.; Geim, A. K.; Morozov, S. V.; Jiang, D.; Katsnelson, M. I.; Grigorieva, I. V.; Dubonos, S. V.; Firsov, A. A. *Nature* **2005**, *438*, 197.
(13) Schniepp, H. C.; Li, J.-L.; McAllister, M. J.; Sai, H.; Herrera-Alonso, M.; Adamson, D. H.; Prud'homme, R. K.; Car, R.; Saville, D. A.; Aksay, I. A. *J. Phys. Chem. B* **2006**, *110*, 8535.
(14) Brodie, B. C. *Philos. Trans. R. Soc. London* **1859**, *149*, 249.
(15) Hummers, W.; Offeman, R. E. *J. Am. Chem. Soc.* **1958**, *80*, 1339.
(16) Boehm, H. P.; Clauss, A.; Fischer, G. O.; Hofmann, U. *Z. Anorg. Allg. Chem.* **1962**, *316*, 119. Boehm, H. P.; Scholtz, W. *Z. Anorg. Alleg. Chem.* **1965**, *335*, 74.
(17) Boehm, H. P.; Scholtz, W. *Z. Anorg. Allg. Chem.* **1965**, *335*, 74.
(18) Lueking, A. D.; Pan, L.; Narayanan, D. L.; Clifford, C. E. B. *J. Phys. Chem. B* **2005**, *109*, 12710.
(19) Fukushima, H.; Drzal, L. T. *Annu. Tech. Conf. − Soc. Plast. Eng.* **2003**, *61*, 2230.
(20) Matsuo, Y.; Higashika, S.; Kimura, K.; Mayamoto, Y.; Fukutsuka, T.; Sugie, Y. *J. Mater. Chem.* **2002**, *12*, 1592.

10.1021/cm0630800 CCC: $37.00
Published on Web 05/25/2007 PAGE EST: 8.4

with strong oxidizers such as sulfuric acid, nitric acid, potassium chlorate, and potassium permanganate. The introduction of oxygen containing functional groups (such as hydroxyl and epoxide) results in an increase in the *d*-spacing of GO as well as a change of hybridization of the oxidized carbon atoms from planar sp^2 to tetrahedral sp^3. To prepare GO, we employ the Staudenmaier oxidation method which uses a mixture of sulfuric acid, nitric acid, and potassium chlorate.[22]

There have been numerous attempts to exfoliate or expand graphite starting with GO or graphite intercalation compounds. Such materials find application in electromagnetic interference shielding,[23] oil spill remediation,[24] and sorption of biomedical liquids.[25] The terms exfoliated and expanded graphite are often used interchangeably.[15−21] Many publications describe the process of making expanded graphite material with accordion- or worm-like structure.[26−28] These materials are not completely exfoliated and contain extensive domains of stacked graphitic layers as depicted by the native graphite X-ray diffraction (XRD) peaks. The majority of these partially exfoliated graphite materials are made by intercalation of graphite with sulfuric acid in the presence of fuming nitric acid.[29−37] The intercalated materials are then heated, and an expansion of the graphite is observed. Although the heating results in a substantial volumetric expansion, the resultant material is described as worm-like or accordion-like, and the typical surface areas (<100 m^2/g)[26] are significantly lower than the theoretical limit of 2630 m^2/g that should be observed if all the graphene surface were exposed.[38] This is due to the domains of retained graphite spacing which results in nonuniform expansion in the *c*-axis.

We originally described the thermal expansion that successfully yields single graphene sheets.[13] In this paper, we expand upon two aspects of the FGS production that contribute to our understanding of the exfoliation process: (i) Although the pressure buildup due to the evolution of gases was shown to be the main mechanism for exfoliation, a fundamental understanding of the kinetics of the decomposition rate and how it compares against the diffusional release of the gases was not provided. (ii) The presence of single graphene sheets was demonstrated, but a statistical analysis of the entire system was lacking. To produce large quantities of FGS consistently, in this paper we focus on these two critical issues. To determine the minimum temperature required for exfoliation, we compare the diffusion rate of evolved gases to the experimentally determined decomposition rate of GO. To quantify the degree of exfoliation, we study the surface area and morphology of the material both in the as-produced dry state and in the solvent-dispersed state and determine the distribution of both the sheet thicknesses and the sheet diameters of the dispersed material.

Experimental Section

Reagents. Natural flake graphite (NFG), sized at 400 μm (grade 3061) and 45 μm (grade 230), was kindly provided by Asbury Carbons (P.O. Box 144, 405 Old Main St., Asbury, NJ 08802). Fuming nitric acid (>90%), sulfuric acid (95−98%), potassium chlorate (98%), and hydrochloric acid (37%) were obtained from Sigma-Aldrich and used as received.

Expansion and Exfoliation of Graphite. GO was prepared according to the Staudenmaier method.[13,22] Graphite (5 g) was reacted with concentrated nitric (45 mL) and sulfuric acid (87.5 mL) with potassium chlorate (55 g). The 500 mL reaction flask was placed in an ice bath, and the potassium chlorate was added slowly over 15 min to avoid sudden increases in temperature. [Caution! Addition of the potassium chlorate results in the formation of chlorine dioxide gas, which is explosive at high concentrations.[39] Purging the head space of the reaction vessel with an inert gas, keeping the reaction vessel cool, and adding the potassium chlorate slowly can help minimize the risk of explosion; however, proper safety equipment including acid resistant gloves, apron, and face shield should be worn while adding the potassium chlorate.] On completion of the reaction, the mixture was added to excess water, washed with a 5% solution of HCl, and then repeatedly washed with water until the pH of the filtrate was neutral. The GO slurry was spray-dried with an inlet air temperature of 300 °C and outlet air temperature of 100 °C, with an air flowrate of 80 kg/h and an atomizer wheel at 25,000 rpm (Niro portable spray dryer, Niro, Inc., 9165 Rumsey Rd., Columbia, MD 21045). The dried sample was stored in a vacuum oven at 60 °C until use. The GO suspension used for microscopy studies was prepared directly from the GO slurry prior to spray-drying. The spacing of the 0002 graphite lattice was monitored using XRD (Rigaku Miniflex diffractometer, Cu K_α radiation, $\lambda = 1.5406$ Å, 9009 New Trails Dr., The Woodlands, TX 77381-5209).

Thermal exfoliation of GO as prepared above was achieved by placing GO (200 mg) into a 25-mm i.d., 1.3-m long quartz tube that was sealed at one end. The other end of the quartz tube was closed using a rubber stopper. An argon inlet was then inserted through the rubber stopper. The sample was flushed with argon for 10 min, and the quartz tube was quickly inserted into a Lindberg tube furnace preheated to 1050 °C and held in the furnace for 30 s.

Oxidized graphite samples were examined by simultaneous thermal gravimetric analysis (TGA) and differential scanning

(21) Stankovich, S.; Piner, R. D.; Chen, X.; Wu, N.; Nguyen, S. T.; Ruoff, R. S. *J. Mater. Chem.* **2006**, *16*, 155.
(22) Staudenmaier, L. *Ber. Dtsch. Chem. Ges.* **1898**, *31*, 1481.
(23) Chung, D. D. L. *Carbon* **2001**, *39*, 279.
(24) Adebajo, M. O.; Frost, R. L.; Kloprogge, J. T.; Carmody, O.; Kokot, S. *J. Porous Mater.* **2003**, *10*, 159.
(25) Kang, F. Y.; Zheng, Y.-P.; Zhao, H.; Wang, H.-N.; Wang, L.-N.; Shen, W.-C.; Inagaki, M. *New Carbon Mater.* **2003**, *18*, 161.
(26) Celzard, A.; Mareche, J. F.; Furdin, G. *Prog. Mater. Sci.* **2004**, *50*, 93.
(27) Chung, D. D. L. *J. Mater. Sci.* **2002**, *37*, 1475.
(28) Lee, S.; Cho, D.; Drzal, L. T. *J. Mater. Sci.* **2005**, *40*, 2001.
(29) Chen, X.-M.; Shen, J.-W.; Huang, W.-Y. *J. Mater. Sci. Lett.* **2002**, *21*, 213.
(30) Chen, X. M.; Shen, J. W. *Acta Polym. Sin.* **2002**, *3*, 331.
(31) Chen, G. H.; Wu, D. J.; Weng, W. G.; Yan, W. L. *J. Appl. Polymer Sci.* **2001**, *82*, 2506.
(32) Chen, G. H.; Wu, D. J.; Weng, W. G.; He, B.; Yan, W. I. *Polym. Int.* **2001**, *50*, 980.
(33) Chen, G. H.; Wu, C.; Weng, W. G.; Wu, D. J.; Yan, W. *Polymer* **2003**, *44*, 1781.
(34) Chen, G. H.; Weng, W. G.; Wu, D. J.; Wu, D. C.; Chen, J. G.; Ye, L. H.; Yan, W. L. *Acta Polym. Sin.* **2001**, *6*, 803.
(35) Chen, G. H.; Wu, D. J.; Weng, W. U. Wu, C. L. *Carbon* **2003**, *41*, 619.
(36) Zheng, W.; Wong, S.-C.; Sue, H.-J. *Polymer* **2002**, *43*, 6767.
(37) Zheng, W.; Wong, S.-C. *Compos. Sci. Technol.* **2003**, *63*, 225.
(38) Peigney, A.; Laurent, Ch.; Flahaut, E.; Bacsa, R.; Rousset, A. *Carbon* **2001**, *39*, 507.
(39) Lopez, M. I.; Croce, A. E.; Sicre, J. E. *J. Chem. Soc., Faraday Trans.* **1994**, *90*, 3391.

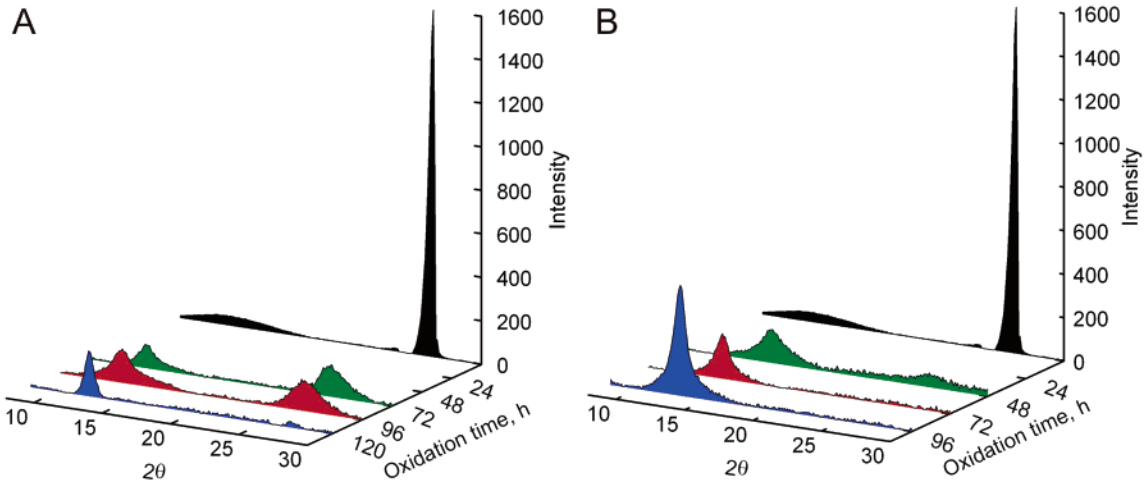

Figure 1. (A) XRD patterns of 400 μm diameter graphite flakes oxidized for various lengths of time. Note that the native graphite peak (between 2θ of 25−30°) persists for oxidation times as long as 96 h. A new peak corresponding to an interlayer spacing of 0.7 nm forms during oxidation. (B) XRD patterns of 45 μm diameter graphite flakes oxidized for various lengths of time. Note the disappearance of the native graphite peak after relatively short oxidation times.

calorimetry (DSC; STA 449 C Jupiter, Erich Netzsch GmbH & Co., Holding KG, D-95100 Selb, Germany). The differential scanning calorimeter was calibrated by a set of standards with known temperatures and enthalpies (In, Sn, Bi, Zn, CsCl). The thermal analysis unit was coupled with a Fourier transform infrared (FTIR) spectrometer for evolved gas analysis (Thermo Nicolet Nexus 670, Thermo Electron Corp., Waltham, MA 02451).

Characterization of Graphite, GO, and FGS. Transmission electron microscope imaging of graphite, GO, and FGS was performed on a JEOL 2010 FEG microscope at 200 keV to characterize especially the variations in the stacking of graphene sheets. The transmission electron microscopy (TEM) samples were prepared by dispensing a small amount of dry powder on 200 mesh copper TEM grids covered with thin amorphous carbon films. The *d*-spacing was calibrated against the interplanar spacing of graphite.

Graphite, GO, and FGS were also characterized by scanning electron microscopy (SEM; Tescan 5130MM, Libusina tr. 21, 62300 Brno, Czech Republic) to determine particle size and microscopic features. SEM samples of GO were prepared by placing a 1 cm-diameter drop of dilute GO suspension on a 1 × 1 cm section of silicon wafer and allowing the solvent to evaporate. The wafer was then attached to an aluminum sample holder with conductive carbon adhesive. The samples were coated with 2−3 nm of iridium to ensure good conductivity. FGS samples for SEM imaging were prepared by applying the powder directly to a carbon adhesive tape.

Imaging of FGS by atomic force micrsocopy (AFM; Multimode, Nanoscope IIIa, Veeco Instruments, Inc., Santa Barbara, CA) was performed with special emphasis on sheet thickness, morphological features, and lateral dimensions. The cantilevers were Veeco NP-S type (gold-coated, oxide-sharpened silicon nitride, force constant $k = 0.58$ N/m, radius of curvature $r = 20$ nm). For the most accurate determination of the sheet thickness, contact mode was applied and topography sections across a sheet, starting and ending on a highly oriented pyrolytic graphite (HOPG) substrate, were taken, following the fast scanning direction. Samples of FGS were prepared by loading a 50 mL flask with 4 mg of graphene and 40 mL of dimethylformamide (DMF) as the dispersion medium. The suspension was ultrasonicated for 30 min. This suspension was diluted to a concentration of 0.02 mg/mL. The final suspension was spin-coated at 5000 rpm on a freshly cleaved surface of HOPG.

Surface area was measured using the Brunauer, Emmett, and Teller (BET)[40] method (Micromeritics Gemini V, One Micromeritics Drive, Norcross, GA 30093) and also in suspension using UV−vis spectroscopy with methylene blue (MB) dye as a probe. Water is the solvent of choice for MB; however, it is a poor dispersant for FGS. Ethanol is a much better dispersant for the FGS suspension but gives a less well-defined peak for MB absorption. We therefore used a combination of the two solvents to make our measurements.

In the MB technique, the surface area measurements were taken by first adding a known mass of FGS to a flask. An amount of MB equal to at least 1.5 times the amount required to cover the theoretical surface area of graphene (2630 m^2/g)[38] was then added. Ethanol was added, followed by sonication with stirring for 1.5 h. The ethanol was then evaporated, and the free MB was redissolved by a known quantity of water. The concentration of MB was subsequently determined by UV−vis spectroscopy relative to standard concentrations. The measurements were made at $\lambda = 298$ nm. Although the reported values of λ_{max} in the literature vary,[41−44] this value is significantly lower than those normally reported, and we expect this was caused by the use of ethanol during the process. The literature value of 2.54 m^2 of surface covered per mg of MB adsorbed was the basis for our calculations.[41] Recent literature reports tend to use a value corresponding to a coverage of 1.30 nm^2 per molecule of MB.[42] However, depending on the assumptions made, the surface coverage of a single MB molecule is reported to range from 1.30 nm^2 for molecules laying flat to 0.66 nm^2 for tilted molecules.[43] For graphite-based samples, flat monolayer coverage is expected.[43,44]

Results and Discussion

Mechanism of Exfoliation. For a successful exfoliation process, we have found it necessary to first increase the *c*-axis spacing by oxidation to 0.7 nm and completely eliminate the 0.34 nm graphite interlayer spacing (Figure 1).[13] The reaction time required to achieve the appropriate level of oxidation for the elimination of the 0.34 nm graphite peak depended on the starting flake size. The reaction progress was monitored by withdrawing aliquots from the reaction

(40) Brunauer, S.; Emmett, P. H.; Teller, E. *J. Am. Chem. Soc*. **1938**, *60*, 309−19.
(41) Rubino, R. S.; Takeuchi, E. S. *J. Power Sources* **1999**, *81*, 373.
(42) Yukselen, Y.; Kaya, A. *J. Geotech. Geoenviron. Eng.* **2006**, *132*, 931.
(43) Pakhovchishin, S. V.; Chernysh, I. G.; Gritsenko, V. F. *Colloid Journal of the USSR* **1991**, *53*, 245.
(44) Sagara, T.; Niki, K. *Langmuir* **1993**, *9*, 831−838.

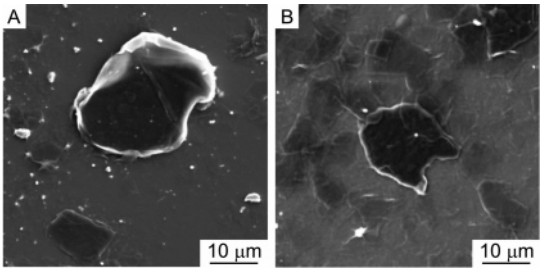

Figure 2. SEM images of GO (A) from 400 μm diameter graphite and (B) from 45 μm diameter graphite. The sizes of the resulting GO flakes are the same order of magnitude regardless of starting graphite flake size.

vessel to be characterized by XRD. The results from studies of two different size flakes, 400 and 45 μm diameter, are shown in Figure 1. From the XRD data, it can be seen that the reaction proceeds more quickly for the 45 μm plates.

During the oxidation process both the 400 and 45 μm graphite flakes break down into smaller GO flakes with sizes on the order of 10 μm in diameter as shown in Figure 2. This final size does not depend on the initial size of the graphite flakes. The oxidative breakup may be facilitated by existing defects as well as a previously proposed cooperative unzipping mechanism.[45] Reducing the starting flake size allows for faster, more reliable oxidation reactions without a significant difference in the final GO flake size.

To determine the composition of the evolved gases that cause the rapid expansion, a series of TGA/DSC experiments were performed where the outlet gas is analyzed by FTIR. A typical TGA/DSC scan of GO along with the FTIR scans performed at varying temperatures is shown in Figure 3. The heating rate had to be kept at or below 1 °C/min to avoid exfoliating the material during the scan. Faster heating rates produce deflagration sufficiently powerful to remove the pan lid and most of the sample from the pan, resulting in inaccurate scans. Small amounts of water are lost during the initial heating stage. At 200 °C, there is a dramatic mass loss accompanied by an exothermic DSC peak. These features correspond to the decomposition of oxygen-containing groups in the GO. The products of this decomposition are found to be CO_2 (wavenumbers 2360 cm^{-1} and 690 cm^{-1}) and H_2O (wavenumbers 1340−1900 cm^{-1} and 3550−4000 cm^{-1}) as expected (Figure 3B).[46] The absence of sulfur, nitrogen, and chlorine-containing compounds indicates that the intercalating species are not present in the washed material and therefore do not participate in the exfoliation. The mass lost during the thermal decomposition is approximately 30% of the initial GO mass.

To estimate the maximum pressure generated by evolved gases, we assume that all of the mass loss is due to carbon dioxide. Because CO_2 has a higher molecular weight than water, this assumption gives us fewer moles of gas and yields a more conservative estimate of the pressure. The pressure of "bulk" CO_2 under the conditions of interest can be estimated from an appropriate equation of state.[47] The calculated pressure ranges from 40 MPa at 200 °C (the decomposition temperature of GO) to 130 MPa at 1000 °C (just below the furnace temperature). However, because the dimensions of the gap in our system are close to the atomic scale, our actual pressure is expected to vary significantly from bulk values. If we assume hard-sphere interactions, we may calculate the pressure using the kinetic theory of gases and taking into account the van der Waals radius of the gas molecules in the collision frequency (Appendix A). In this case, the calculated pressures are in excess of 200 and 600 MPa at 200 and 1000 °C, respectively.

To calculate the pressure required to exfoliate GO, we consider GO as a multilayer system and apply Lifshitz's formulation of van der Waals forces to calculate the binding energy between two adjacent layers.[48] The pressure needed to overcome van der Waals binding is given by

$$P = \frac{\partial G}{\partial l} = \frac{A_{\mathrm{Ham}}}{6\pi l^3} \tag{1}$$

where G is the interaction free energy per unit area between two semi-infinite slabs, A_{Ham} is the Hamaker coefficient, and l is the interlayer distance. Because the van der Waals binding force is inversely proportional to l^3 and the pressure generated from evolved gases is inversely proportional to l, once the exfoliation process in GO is initiated, the multilayer binding is ruptured at an accelerating pace. By numerically evaluating the Hamaker constant, we estimate the pressure required to separate two GO sheets to be 2.5 MPa (Appendix B). Our estimates of the pressures generated during exfoliation are 1−2 orders of magnitude greater than the van der Waals forces binding the GO sheets together.

The above pressure calculations are performed assuming that the gas cannot escape the inter-lamellar region of GO before the expansion occurs. The diffusion time scale calculated from Knudsen diffusion is on the order of 10^{-4} s. On the basis of the TGA observations, at heating rates of 1 °C/min or less, diffusion of the evolved gases is sufficient to avoid exfoliation. Figure 4 shows the XRD data for graphite, GO, FGS, reduced GO that has been produced by slowly heating GO at a rate of 1 °C/min to 1050 °C, and FGS. Note that the d-spacing for the slowly reduced GO sample reappears at a value very close to the native graphite values for the 0002 peak and the stacking is retained while a broad peak corresponding to the 0.7 nm GO interlayer separation is partially retained. Relative to native graphite, the peak at $2\theta \approx 27°$ is now broad, presumably because of the corrugated structure of the GO sheets. The van der Waals forces are sufficient to maintain graphitic stacking if gas evolution, and expansion occur slowly enough that lateral diffusion can relieve the generated pressure.

The conservation equation for diffusion only in the radial direction in cylindrical coordinates reduces to eq 2,

$$\frac{\partial C_i}{\partial t} = D_i \frac{1}{r} \frac{\partial}{\partial r}\left(r \frac{\partial C_i}{\partial r}\right) + R \tag{2}$$

where C_i is the concentration of species i, t is time, D_i is the

(45) Li, J.-L.; Kudin, K. N.; McAllister, M. J.; Prud'homme, R. K.; Aksay, I. A.; Car, R. *Phys. Rev. Lett.* **2006**, *96*, 176101.
(46) Rodriguez, A. M.; Jimenez, P. V. *Thermochim. Acta* **1984**, *78*, 113.
(47) Span, R.; Wagner, W. J. *Phys. Chem. Ref. Data* **1996**, *25*, 1509.
(48) Parsegian, V. A. v*an der Waals Forces: A Handbook for Biologists, Chemists, Engineers, and Physicists*; Cambridge University Press: New York, 2005.

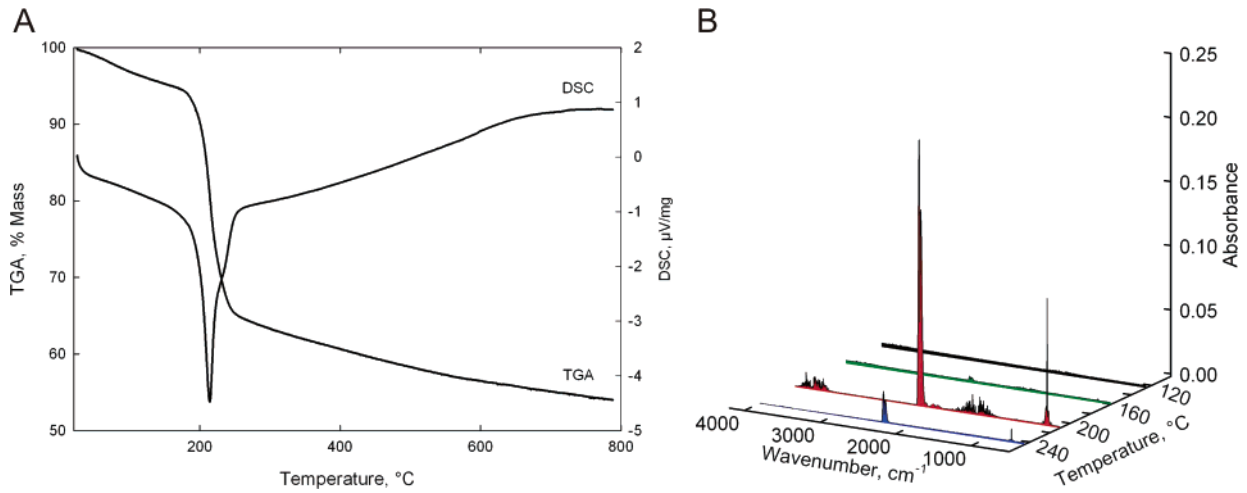

Figure 3. (A) TGA/DSC scans of GO. There is a sharp mass loss at an onset temperature of approximately 200 °C accompanied by a strongly exothermic DSC peak. (B) FTIR scans of the evolved gas from the TGA of GO. The strongest signal present is that of CO_2 (wavenumbers 2360 cm^{-1} and 690 cm^{-1}) and H_2O (wavenumbers 1340−1900 cm^{-1} and 3550−4000 cm^{-1}) just after the onset of rapid mass loss. This indicates that decomposition of the oxygen-containing functional groups, rather than vaporization of intercalants, causes the exfoliation.

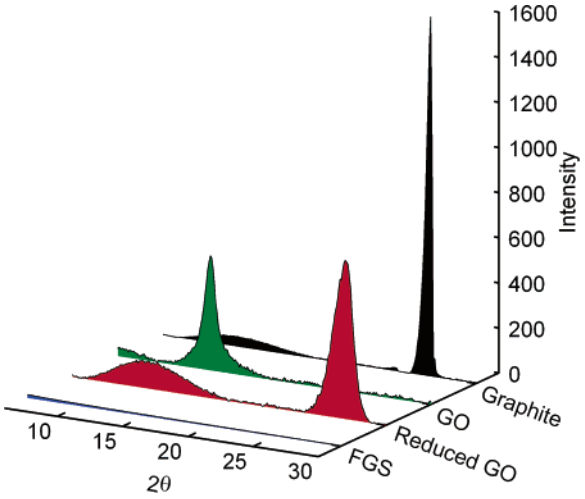

Figure 4. XRD patterns of graphite, GO, GO that has been thermally reduced by slow heating (1 °C/min), and FGS. When GO is heated slowly, the rate of gas evolution is insufficient to yield high enough pressures to overcome the van der Waals attraction between the layers and with removal of the functional groups the layers restack to roughly the initial graphite spacing. FGS displays an amorphous structure pattern.

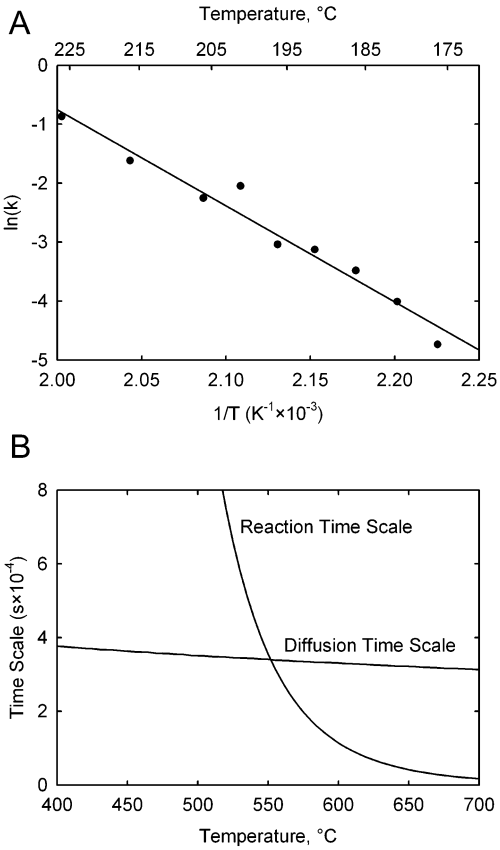

Figure 5. (A) Arrhenius plot of GO decomposition data. (B) Plots of the reaction time scale and diffusion time scale as a function of temperature.

diffusivity of species i, r is the radial position, and R is the rate of formation of the gaseous species. Because the pressure in the system is directly related to the concentration of the gas, to accumulate pressure in the system $\partial C_i/\partial t$ must be large enough to overcome the van der Waals forces holding the GO sheets together. Through a simple scaling analysis, the diffusion time scale is calculated as r_p^2/D_i where r_p is the radius of a GO platelet.

To determine the critical temperature at which the reaction time scale is shorter than the diffusion time scale, we monitor the isothermal decomposition of GO at varying temperatures using TGA. The experimental data are reported in Figure 5A and follow Arrhenius behavior. Temperatures above 230 °C cannot be investigated for GO using this technique, as attempts to do so cause an exfoliation during the heating stage. The decomposition data follow second-order kinetics with respect to oxygen content. We then estimate the reaction time scale as $1/[k(1 - x)]$ where x is the fractional conversion of oxygen chemically bound to the GO and k is the reaction rate constant. The total mass loss of GO upon heating is determined by TGA (Figure 3), and the fractional conversion is the mass evolved relative to the total mass loss. For this scaling analysis, we use the initial concentration of functional groups, where the fractional conversion is zero. With the kinetic parameters thus determined, we plot the reaction time scale and the diffusion time scale as shown in Figure 5B. We see that at a temperature of 550 °C the reaction time scale is shorter than the diffusion time scale. This temperature is outside the experimentally available data range, so this extrapolation should be regarded as an estimate. The energy

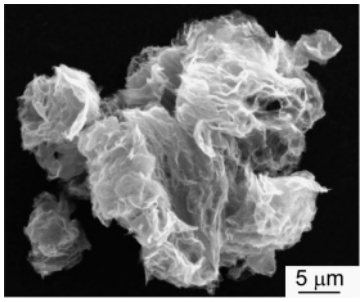

Figure 6. SEM image of dry, as-produced FGS powder. The sheets are highly agglomerated, and the particles have a fluffy morphology.

evolved during the exfoliation is determined by integrating the DSC peak relative to known standards. The heat of reaction was found to be 1500 J/g of GO (or, alternatively, 5000 J/g of gas evolved). A conservative estimate of an adiabatic temperature rise of 750 °C was found by dividing the heat of reaction by the heat capacity of GO, which was assumed to be similar to that of graphite (2 J/(g·K)).[49] Because the heat capacity of a material is a function of temperature, we have used the highest heat capacity over the range of interest for this estimate. Because the external heating rate is limited by the thermal diffusivity of GO, this strong internal heating ensures the samples exceed the critical temperature of 550 °C during the decomposition.

Degree of Exfoliation. The degree of exfoliation of GO has been characterized using two separate surface area measurement techniques as well as SEM, TEM, XRD, and AFM. The XRD pattern of FGS, shown in Figure 4, indicates an amorphous structure. While this does not necessarily require that all stacking is lost, it does indicate that any remaining stacking is disordered. As we have demonstrated, this disruption of the structure and the *d*-spacing greatly reduces the attractive interactions between the layers, allowing this material to be easily dispersed in solvents.

A representative SEM image of the dry, as-produced FGS powder is shown in Figure 6. What is observed is an agglomerated powder with a "fluffy" appearance which contrasts previous work of others in which a worm-like (or vermiculite) structure was observed.[26−28] After dispersing the sheets in solvent using ultrasonication, SEM was no longer the best technique to use as this fluffy appearance was replaced by a wrinkled thin paper-like structure (Figure 7C). We then relied on TEM and AFM for high-resolution characterization.

High-resolution transmission electron microscopy (HRTEM) images of graphite, GO, and FGS are shown in Figure 7. Congruent with the XRD results, the edge-on HRTEM image of graphite (Figure 7A) shows a characteristic inter-graphene spacing of 0.34 nm. Also congruent with the XRD data, the edge-on image of GO (Figure 7B) shows an inter-graphene spacing of roughly double the spacing of graphite. Graphene sheets of GO are corrugated, but the selected area electron diffraction (SAED) pattern in the inset indicates a crystalline structure. The SAED pattern contains information from many GO grains. A typical sharp, polycrystalline ring pattern is obtained. The first ring comes from

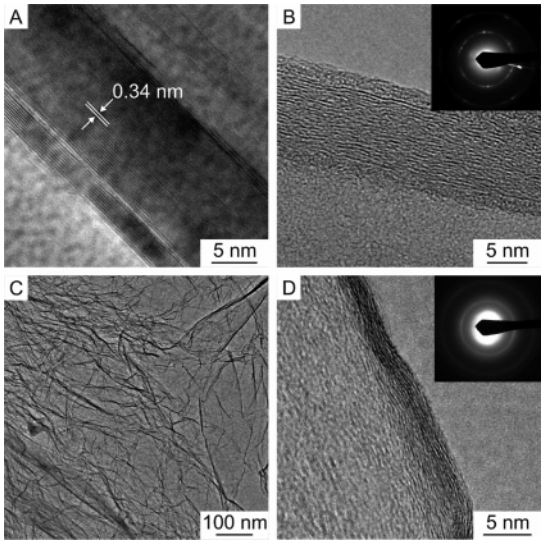

Figure 7. (A) HRTEM image of graphite showing its characteristic 0.34-nm interlaminar spacing. (B) HRTEM image illustrates the intercalation of GO samples oxidized for more than 96 h. The GO sheets are wrinkled compared to that of pristine graphite. The SAED pattern in the inset contains information from many GO grains. (C) TEM image of FGS. (D) An edge-on HRTEM image of FGS produced from GO with a 96-h acid treatment showing a multi-stack region.

the (1100) plane, and the second ring comes from the (1120) plane. Strong diffraction spots are observed on the ring. The bright spots corresponding to the (1100) reflections within the ring retain the hexagonal symmetry of the [0001] diffraction pattern. These results imply that the GO sheets before thermal treatment are not randomly oriented with respect to one another, and the interlayered coherence is not destroyed at this stage. The corrugation of the GO sheets is attributed to the disruption of the planar sp^2 carbon sheets by the introduction of sp^3-hybridized carbon upon oxidation. This corrugated structure is also consistent with the line broadening observed in the XRD patterns (Figures 1 and 4).

The TEM images of the as produced dry FGS powder, similar to the one in Figure 6, show a wrinkled paper-like structure in low magnification (Figure 7C). Because this powder was not yet dispersed in solvent, the HRTEM images of some regions from an edge-on view show stacks of graphene sheets arranged with a disordered structure in the bulk of the stack. In Figure 7D, only in the outer region a structure similar to that of GO (Figure 7B) is observed. The SAED pattern in the inset of Figure 7D shows only weak and diffuse rings, indicating the loss of long range ordering between the graphene sheets. The stacking of the sheets due to van der Waals attractive interactions, even with a random arrangement, is expected.

AFM characterization has been the most direct method of quantifying the degree of exfoliation to a single graphene sheet level after the dispersion of the powder in a solvent. We have previously confirmed the presence of single-sheet graphene using this oxidation/exfoliation mechanism by AFM.[13] In this previous study, suspensions of FGS were centrifuged to facilitate sample preparation, whereas in the present study, the sample is not fractionated in any way in an attempt to determine what fraction of the sample is composed of single sheets. The minimum measured height

(49) Butland, A. T. D.; Maddison, R. J. *J. Nucl. Mater.* **1973**, *49*, 45.

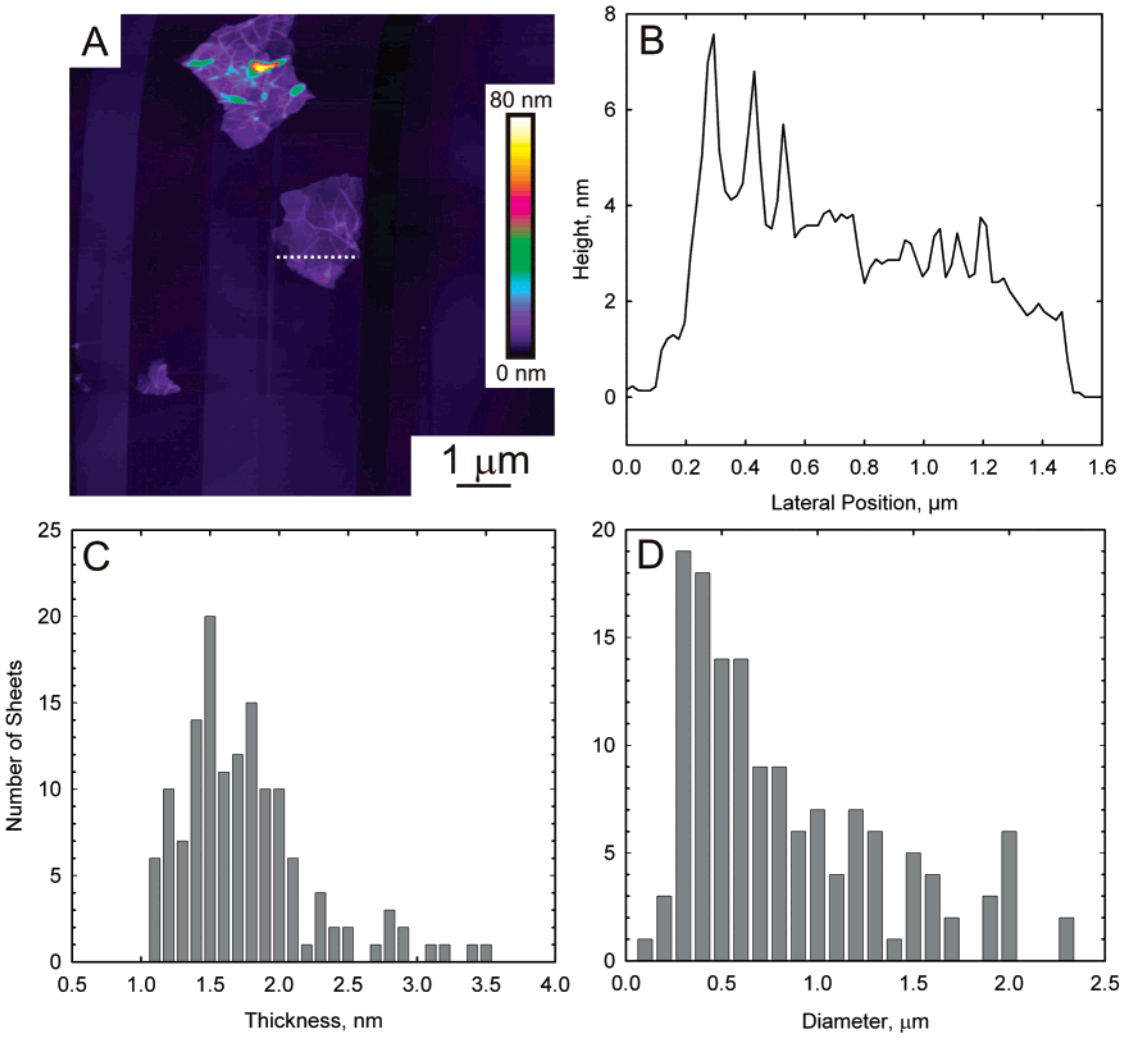

Figure 8. (A) Contact-mode AFM scan of FGS deposited on a freshly cleaved HOPG surface. (B) Height profile through the dashed line shown in part A. (C) Histogram of sheet thicknesses from images of 140 sheets. The mean thickness is 1.75 nm. (D) Histogram of sheet diameters from the same 140 sheets. No correlation between diameter and thickness could be discerned.

of each sheet was taken as the thickness because the wrinkled sheets only come into close contact with the substrate at a few points (Figure 8A, B). This would not account for any space between the sheet and the substrate or if the radius of curvature of the AFM tip is too large to access the actual minimum height. These thickness measurements should be viewed as an upper bound of the actual thickness of the sheets. The thicknesses of 140 sheets were measured, and the histogram is shown in Figure 8C. The minimum sheet thickness is 1.1 nm, and the mean is 1.75 nm. This is very similar to what was found previously for the centrifuged sample.[13] The first significant difference that we find here is that there are a number of sheets that have a measured thickness that is greater than one standard deviation from the mean. If we assume that none of the sheets in this range can be individual graphene sheets, we find that roughly 80% of the investigated material consists of single sheets. The other significant difference is that centrifugation also removed the large diameter single sheets that we have retained here. The histogram for the diameters is shown in Figure 8D. There are sheets as small as 100 nm and as large as 2.5 μm, while the centrifuged sample only contained sheets on the order of hundreds of nanometers. Figure 8A shows an AFM scan of three different sheets. Two are single sheets of varying sizes; the third object is much thicker and is assumed to be a multilayered sheet similar to one displayed in TEM image of Figure 7D. Interestingly, there is no correlation between sheet thickness and diameter.

Surface areas measured using the BET method by nitrogen gas adsorption ranged from 600 to 900 m^2/g. Variations observed within a single batch suggested that BET surface areas determined on dry powders are affected by the state of agglomeration of the powder. To measure the surface area of dispersed material, the graphene surface area was determined in an ethanol suspension with MB dye as a probe. Batches of functionalized graphene that had typical surface areas ranging from 600 to 700 m^2/g by BET showed surface areas of 1,850 m^2/g using the MB adsorption technique.

Although the theoretical surface area of graphene is 2630 m^2/g,[38] this surface area would only be observed in a hypothetical case where no overlap of sheets exists. In a real system, a significant amount of surface area is not available for nitrogen or dye adsorption because of overlap of the exfoliated sheets. Furthermore, a dry system would have less

surface available than a solvent dispersed system as the solvent acts to help maintain separation and limit agglomeration of the sheets. This is what is observed experimentally.

Conclusions

We have investigated the exfoliation mechanism and performed sample characterization of exfoliated graphite to determine the important parameters for successful and consistent exfoliation. Smaller 45 μm graphite flakes are intercalated and oxidized within 96 h with a high degree of reliability, while larger 400 μm graphite flakes can take over 120 h and regularly fail to fully intercalate and oxidize. There is no significant size difference in the GO product as we change the size of the starting graphite flakes, which suggests that the product size is intrinsically determined by the oxidation process. The gaseous products are derived from the exothermic decomposition of hydroxyl and epoxide groups of the GO prepared by Staudenmaier's method, not from the vaporization of intercalated species. This proves to be an important distinction, as the thermal energy evolved in the decomposition locally heats the sample allowing for faster reaction rates and higher internal temperatures, ensuring sufficient rapid pressure buildup for uniform exfoliation. The dry FGS powders are highly agglomerated, as evidenced by the BET surface area and SEM characterization. Unlike graphite or GO, however, FGS is easily dispersed in solvents by ultrasonication as evidenced by the MB surface area and AFM characterization of the dispersed sheets. Thus, the BET surface area does not provide a consistent and accurate means to assess the degree of exfoliation of the material but rather only gives a rough estimate of the state of the material. The dispersed material consists of at least 80% single graphene sheets.

Acknowledgment. Financial support from the NASA University Research, Engineering, and Technology Institute on BioInspired Materials (BIMat) under Award No. NCC-1-02037 and the National Science Foundation NIRT under Grant No. CMS-0609049 is greatly appreciated. We thank Daniel M. Dabbs for his assistance in the preparation of the manuscript.

Appendix A: Calculation of Generated Pressure

To estimate the maximum pressures that could be generated by the evolution of CO_2, we first assume that all of the available CO_2 is released and remains contained within the galleries of GO and that the GO spacing does not change. We next assume that the functional groups are homogeneously distributed so that each gallery has available half of the oxygen from each neighboring sheet which is equal to the amount of oxygen bound to any individual sheet as epoxide and hydroxyl sites (Figure 9). To estimate the total volume between the layers per mass of GO, we take the center-to-center layer distance from XRD of 0.71 nm and subtract the thickness of the graphene sheets of 0.34 nm which gives a spacing of 0.37 nm. We divide this distance by the planar density of an individual graphene sheet, calculated from the unit cell of graphite to give the interlayer volume per mass of GO. We then use the TGA data to determine the mass of CO_2 generated per mass of GO. By dividing the mass of CO_2 generated per mass GO by the total gallery volume per mass GO and converting to a molar basis, we find a CO_2 density of 9300 mol/m^3 which is used to calculate pressures at varying temperatures.

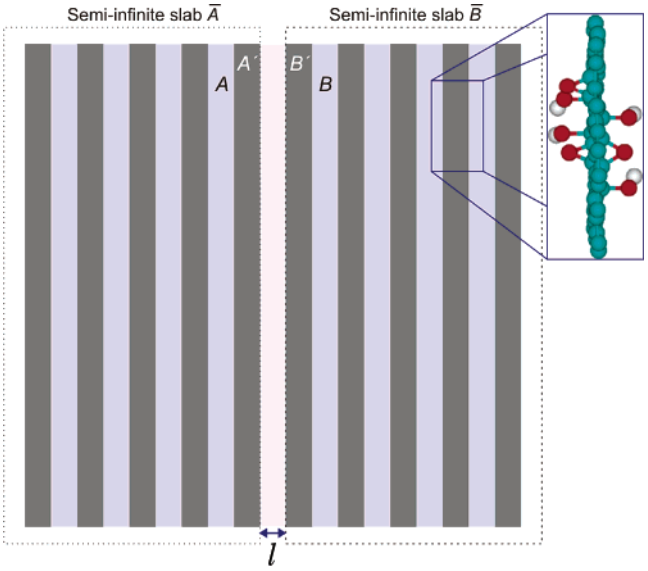

Figure 9. GO is modeled as a multilayer system. Two semi-infinite slabs $\bar{A}$ and $\bar{B}$ are separated by a distance l, and both are composed of alternating layers of graphene sheets (A' and B') whereas empty regions (A and B) are pillared by oxygen-containing (epoxy and hydroxyl) functional groups as shown in the enlarged area.

The force exerted on the surface of interest is calculated as $F = Nm\bar{u}_x^2/x$ where N is the number of particles, m is the particle mass, $\bar{u}_x^2$ is the mean square velocity component normal to the surface, and x is half of the round-trip distance between collisions with the same wall. We assume that the motion of the particles is random so that $\bar{u}_x^2 = {}^1/_3\bar{u}^2$ where $\bar{u}^2$ is the mean-square velocity approximated by $3k_BT/m$ where k_B is the Boltzmann constant, T is the temperature, and m is the mass of the particle. Again we use the distance as 0.37 nm and subtract twice the van der Waals radius of a carbon atom (the largest atom in the CO_2 molecule) to obtain $x = 0.06$ nm. If we neglect the size of the molecules, this calculation gives the ideal gas law. We note that CO_2 is a linear molecule that must lie parallel to the planes of the graphene sheets at the separation distance observed. Limiting the rotational freedom of the molecules could cause the pressure to diverge from the ideal case to an even greater extent than calculated here.

Appendix B: Pressure Calculation due to van der Waals Forces

We consider GO as a multilayer system composed of hydrocarbon[50] sheets. The functional groups on GO act like spacers so that the thickness of the hydrocarbon sheet is b'

(50) Typical Hamaker coefficients of carbon-based insulators are similar, i.e., A_{Ham} does not vary much for different hydrocarbons. Therefore, we can use a typical dielectric screening function of hydrocarbon in the evaluation of Hamaker coefficients in GO. We model the dielectric function of the B' sheets with the simple expression $\epsilon_{B'}(\omega) = 1 + 1/(1 - (\omega/\omega_{hc})^2)$ where we take $\omega_{hc} = 1.5 \times 10^{16}$ rad/s. Mahanty, J; Ninham, B. W. *Dispersion Forces*; Academic Press, New York, 1976.

$= 0.34$ nm and the interlayer separation $b = 0.37$ nm (Figure 9). The exfoliation process is initiated at a particularly weak interlayer spacing susceptible to rupture due to gas pressure. The pressure needed to overcome van der Waals binding is given by

$$P = \frac{\partial G}{\partial l} = \frac{A_{\mathrm{Ham}}}{6\pi l^3} \tag{B1}$$

where $l = 0.37$ nm is the spacing between two semi-infinite GO slabs. We use Lifshitz's theory of van der Waals forces in the non-retarded regime (i.e., the speed of light $c = \infty$). Following the formulation of the effective Hamaker coefficients of a multilayer system (see pp 297−300 of ref 48), the numerical evaluation of the effective Hamaker coefficient yields

$$A_{\mathrm{Ham}} = 2.37 \times 10^{-21}\ \mathrm{J} \tag{B2}$$

and the pressure in eq B1 is

$$P = 2.49 \times 10^{6}\ \mathrm{Pa} \tag{B3}$$

In the above treatment, we regard GO as a multilayer system composed of insulating sheets. If the layers A' and B' are treated as graphene, an anisotropic conducting material, the required pressure is increased to 7.2×10^6 Pa, about 2.9 times larger than the value given above. We note even at such extreme conditions, it is still smaller than the pressure generated by CO_2 and water during the exfoliation process.

Appendix C: Knudsen Diffusion

To estimate the diffusion time scale, we recognize that the mean free path of the CO_2 molecules is determined by the GO layer spacing, allowing us to utilize the equation for Knudsen diffusion in a slit pore as shown in eq C1[51]

$$D = \left[\frac{4l}{3}\left(\frac{w}{2l + w}\right)\right]\left(\frac{8RT}{\pi M}\right)^{1/2} \tag{C1}$$

where D is the diffusion coefficient, l is the gap height, w is the gap width, R is the gas constant, T is absolute temperature, and M is the molecular weight of the diffusing gas. In the limit that $w \gg$ h, the term $(w/2h + w)$ goes to 1 such as in our case. We define the diffusion time scale in terms of the characteristic diffusion length r_D such that $\tau_D = r_D^2/D$. The diffusion length is taken to be the radius of the flake-like particles.

CM0630800

(51) Bach, H. T.; Meyer, B. A.; Tuggle, D. G. *J. Vac. Sci. Technol., A* **2003**, *21*, 806.